INFLUENCE OF AL COMPOUND AND GYPSUM ADDITION ON TOBERMORITE FORMATION IN HYDROTHERMALLY TREATED CEMENT-BASED MATERIALS STUDIED BY *IN SITU* X-RAY DIFFRACTION

KUNIO MATSUI[1*], AKIHIRO OGAWA[1], JUN KIKUMA[2], SHINYA MATSUNO[2]

[1]*Asahi-KASEI Construction Materials Corporation*
106 Someya Sakaimachi, Sashimagun, Ibaraki 306-0493, Japan.
**E-mail: matsui.kj@om.asahi-kasei.co.jp*
[2]*Analysis and Simulation Center, Asahi-KASEI Corporation*

ABSTRACT

Hydrothermally treated cement-based materials are widely used in buildings because such materials have high durability and fire resistance. It has been reported that both the quantity and quality of tobermorite ($5CaO \cdot 6SiO_2 \cdot 5H_2O$) formed in these materials considerably affect their mechanical properties. We have therefore investigated the formation of tobermorite during hydrothermal processing by *in situ* X-ray diffraction analysis using high-energy X-rays from a synchrotron radiation source. Specifically, the effects of Al and gypsum addition on tobermorite formation were studied. Acceleration of tobermorite formation by Al and gypsum addition was clearly observed. In an experiment on gypsum addition, the Avrami model fitted well to the calculated reaction degrees over almost the entire reaction period, and different exponent coefficients were obtained for the systems with and without gypsum. The tobermorite formation mechanisms in these systems were also examined.

KEYWORDS:

In situ X-ray diffraction, tobermorite, hydrothermal, cement, gypsum

INTRODUCTION

Hydrothermally treated cement-based materials are widely used in buildings because such materials have high durability and fire resistance. In particular, autoclaved aerated concrete (AAC) has attracted attention as a hydrothermally treated cement-based material because of its excellent heat insulation properties (Grutzeck, 2005; Haas, 2005). A typical process for the production of AAC includes hydrothermal treatment of a mixture of quartz sand, lime, cement, gypsum and other additives at high temperature (typically, 180–200 °C) under saturated steam pressure, which results in the formation of crystalline calcium silicate hydrate, namely, tobermorite ($Ca_5Si_6O_{16}(OH)_2 \cdot 4H_2O$). Since both the quantity and quality of tobermorite formed in AAC considerably affect its mechanical properties (Mitsuda *et al.*, 1992), understanding the mechanism of tobermorite formation during hydrothermal treatment (i.e., the autoclave process) is important in AAC production. The synthesis of tobermorite under hydrothermal conditions has been extensively studied for various starting materials including several types of silica sources and various additives. It has been revealed that Al compounds and gypsum significantly affect the tobermorite formation process (Larosa-Thompson *et al.,* 1996; Sakiyama *et al.*, 2000). However, this process is more complex in industrial AAC production because of the various impurities in the raw materials. Therefore, the formation mechanism of tobermorite is not thoroughly understood for such processes.

We have developed a relatively large autoclave cell for *in situ* transmission X-ray diffraction (XRD) analysis, which has sufficient space for the sample and the water reservoir. Through this analysis, the formation process

of tobermorite from cement-based starting materials has been successfully observed (Kikuma *et al.*, 2010, 2011; Matsui *et al.,* 2011). In the present study, we applied this method to the AAC autoclave process, and the effects of Al compound and gypsum addition on the tobermorite formation reaction in AAC production were investigated.

EXPERIMENTAL

Materials and Sample Preparation

The compositions of the starting materials are listed in Table 1. Two types of crushed quartz were used as silica sources: (A) quartz rock (purity >96.9%) and (B) quartz sand (purity >96.8%). High-early-strength Portland cement (HPC) was purchased from Ube-Mitsubishi, Ube, Japan. γ-Al_2O_3, quicklime and gypsum were research grade. Mixtures composed of the starting materials were fully mixed in the presence of water at 50 °C. The water-to-solid ratio was 0.75 by weight. For each run, the slurry mixture was poured into a plastic beaker and kept at 60 °C for more than 12 h for the cement in the mixture to become hydrated. The hydrated mixture was then cooled, and was cut into specimens with dimensions of 6 mm × 18 mm and thickness of 3.0 mm, immediately before the *in situ* measurement was conducted. In this study, we did not use a foaming agent (e.g., Al metal powder), which is generally used in the AAC process, to avoid nonuniformity of X-ray transmission in the samples.

Table 1 - Composition of starting materials

Experiments		Al addition		gypsum addition	
Samples		A (without Al)	B (with Al)	C (without gypsum)	D (with gypsum)
Quartz (type)	(mass %)	54.4 (quartz A)	51.5 (quartz A)	55.7 (quartz B)	53.5 (quartz B)
Quicklime	(mass %)	4.7	4.9	5.4	5.1
HPC	(mass %)	38.9	38.9	38.9	37.4
Gypsum	(mass %)	2.0	2.0	0	4.0
γ-Al_2O_3	(mass %)	0	2.7	0	0
Ca/(Si+Al)	(molar ratio)	0.51	0.51	0.51	0.51
Al/(Si+Al)	(molar ratio)	0.037	0.088	0.037	0.037

In Situ XRD Measurement

XRD measurements were carried out at the BL19B2 beamline of SPring-8 in Japan using an X-ray energy of 30 keV. The X-ray energy was selected so that the transmittance of X-rays through the sample would be around 50%. The temperature of the autoclave cell was controlled by a copper heater block surrounded by a thermal insulator. First, the temperature was raised to 100 °C at a ramping rate of 2 °C/min. The temperature was held at 100 °C for 15 min. During this period, the cell was evacuated for a few seconds, and about 95% of the air was removed from the cell. After the steam pressure was built up again at 100 °C, the first XRD measurement was conducted. After 15 min at 100 °C, the temperature was raised to 190 °C at a ramping rate of 1 °C/min, and then held at 190 °C for 12 h. During this process, the XRD measurements were conducted using a photon-counting pixel array detector, PILATUS 100K (DECTRIS, Baden, Switzerland). The measurement interval was 4.25 min. During the exposure time, the cell, together with the heater block, was

oscillated in the vertical direction at an amplitude of 3.0 mm and a rate of 0.6 mm/s to average the measurements over a larger area of the sample.

Analysis of Non-Crystalline Phase

In the present *in situ* experiment, we were able to observe the intensity change in an amorphous halo at around 3.4 nm^{-1}, where the halo of non-crystalline calcium silicate hydrate (C-S-H) is observed. Non-crystalline C-S-H is formed by hydration of cement and is well-known as a major precursor to tobermorite formation. The integrated intensity from 3.427 to 3.434 nm^{-1} was regarded as the C-S-H intensity in our previous studies (Kikuma *et al.,* 2010, 2011; Matsui *et al.,* 2011). In the present study, this method was used to estimate the quantity of C-S-H.

RESULT AND DISCUSSION

Phase Evolution in Experiments on Al Addition

Figure 1 shows the time-resolved XRD data set for the sample without Al addition. Several constituents involved in the reaction are clearly observed. Time profiles of the relative peak intensity of each major constituent for samples without and with Al addition are plotted in Figs. 2(a) and (b), respectively. The sum of the (211) and (002) peak intensities for hydroxylellestadite (HE: $Ca_{10}(SiO_4)_3(SO_4)_3(OH)_2$), and the sum of the (211) and (220) peak intensities for katoite (KA: $Ca_3Al_2(SiO_4)_{3-x}(OH)_{4x}$; x = 1.5–3.0), which is a type of hydrogarnet, are plotted to obtain larger peak integrals and better statistics. For tobermorite, the (002) and (220) peaks are separately plotted. All data are normalized on the basis of XRD measurements of the same sample in our laboratory after *in situ* XRD.

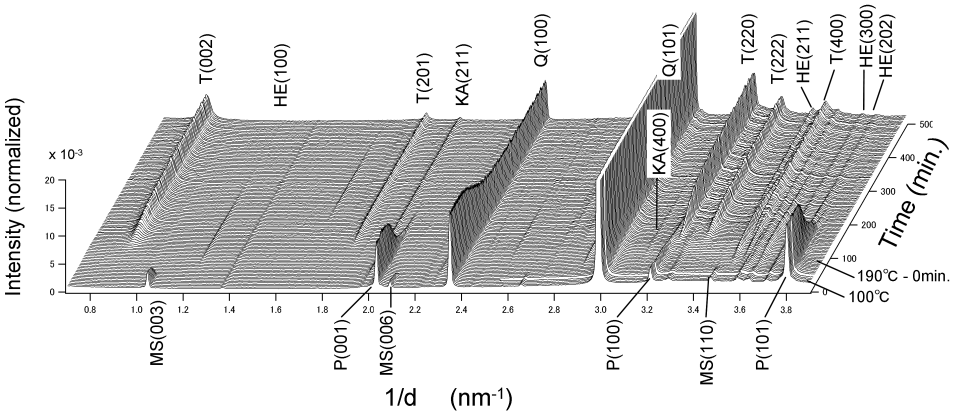

Fig. 1 Stack of time-resolved XRD patterns for sample without Al addition. Temperature was raised from 100 to 190 °C and held at 190 °C. T, tobermorite; P, portlandite; Q, quartz; MS, monosulfate; KA, katoite; HE, hydroxylellestadite.

In these two experiments, monosulfate (MS: $Ca_4Al_2O_6(SO_4)\cdot 14H_2O$) and portlandite (P: $Ca(OH)_2$) were observed at the beginning of the autoclave process. Their intensities then decreased as the reactions proceeded before completely disappearing. Quartz initially decreased slowly; the rate of decrease then became slightly

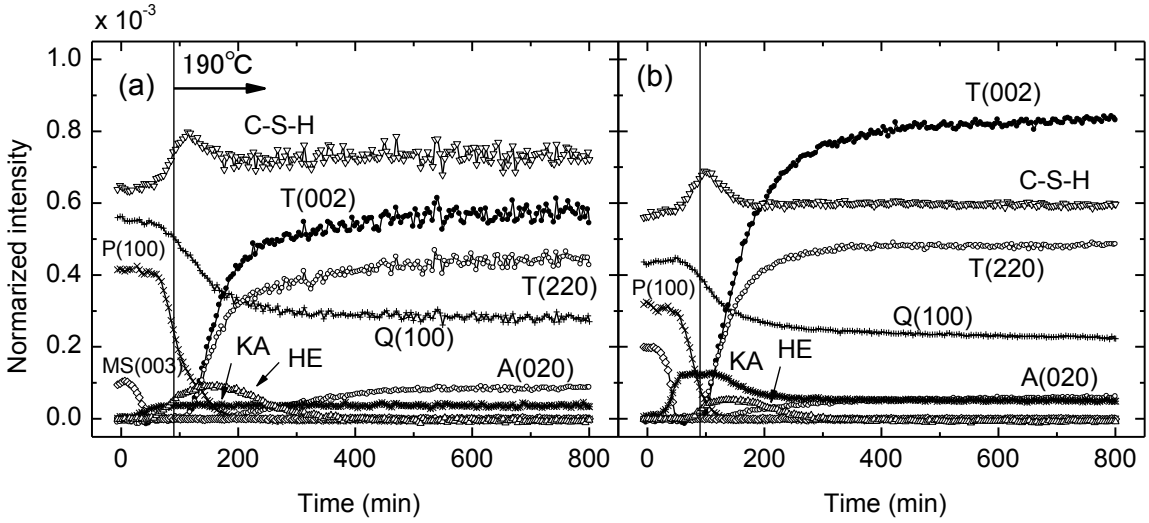

Fig. 2 Time profile of peak intensity for each major constituent during autoclave process: (a) sample without Al addition and (b) sample with 5 mol % Al addition.

faster in the middle stage before slowing again toward the end of the process. As intermediate phases, KA and HE were observed in the middle of the reactions. In the later stage, HE decreased and disappeared, whereas KA decreased slowly and partly remained. Tobermorite began to be observed after the temperature reached 190 °C, at which point the C-S-H intensity was at its peak. The tobermorite formation then increased toward the end of the autoclave process. Anhydrite (A: $CaSO_4$) was initially observed when HE was at its maximum value, and then increased gradually until the end. This suggests that SO_4^{2-} ions released from HE are involved in anhydrite formation.

Tobermorite Formation via C-S-H and KA

As shown in Fig. 2, Al addition accelerated crystallisation of tobermorite, especially in the c-axis (002) direction, On the other hand, C-S-H and KA exhibited unique behaviour with Al addition. To clarify this point, the relation between C-S-H and tobermorite intensity is plotted in Fig. 3, and the relation between KA and tobermorite intensity is plotted in Fig. 4. It can be seen from both figures that after the temperature reached 190 ºC, C-S-H and KA (with Al addition) decreased with increasing intensity of tobermorite. This suggests that there are at least two pathways to tobermorite formation, namely, the C-S-H route and the KA route. For the C-S-H behaviour shown in Fig. 3, the amount of remaining C-S-H (length of vertical arrow) was decreased by Al addition. In other words, tobermorite formation via C-S-H was accelerated by Al addition. Consequently, the main route of tobermorite formation may shift from the C-S-H route to the KA route.

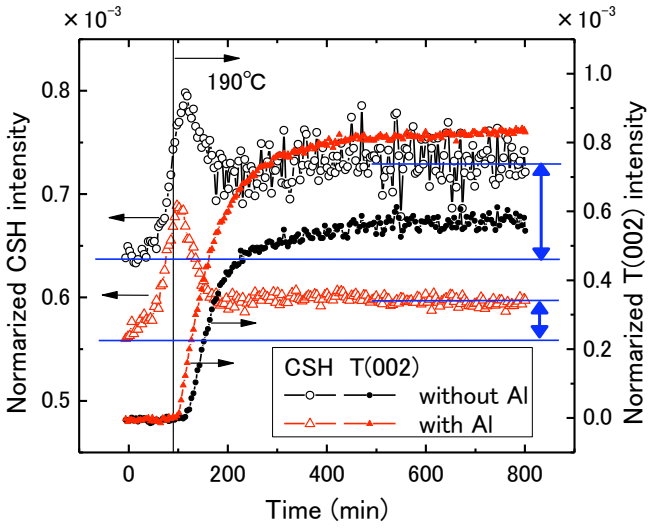

Fig. 3 Time profiles of C-S-H and tobermorite (002) intensities for samples without Al addition and with 5 mol % Al addition.

Phase Evolution in Experiments on Gypsum Addition

The time profiles of the relative peak intensity of each major constituent for samples without gypsum addition and with 4 mass % gypsum addition are plotted in Figs. 5(a) and (b), respectively. For both samples, the start of tobermorite formation corresponded to the maximum C-S-H intensity, and the tobermorite intensity increased with decreasing C-S-H intensity. It is reasonable to consider that the majority of the tobermorite phase was formed via the C-S-H phase, in the same manner as for Al addition. Tobermorite formation began earlier in the sample with gypsum addition than in the sample without gypsum addition. Furthermore, the tobermorite formation rate was higher in the initial stage of the reaction with gypsum addition. It was clearly observed that MS, HE and anhydrite intensities became stronger due to the increased concentration of SO_4^{2-} from the gypsum (Fig. 5(b)). In this system, the maximum HE intensity coincided with the starting point of anhydrite formation. Several studies have reported that HE decomposes into anhydrite and tobermorite under hydrothermal processing (Sakiyama *et al.,* 2000). Our results are consistent with these studies. Therefore, tobermorite formation via HE is considered to be an important reaction route in addition to the above mentioned KA and C-S-H routes.

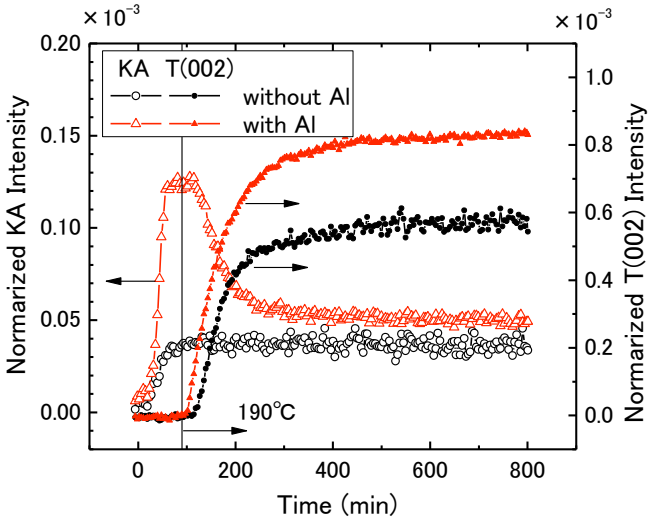

Fig. 4 Time profiles of KA (katoite) and tobermorite (002) intensities for samples without Al addition and with 5 mol % Al addition.

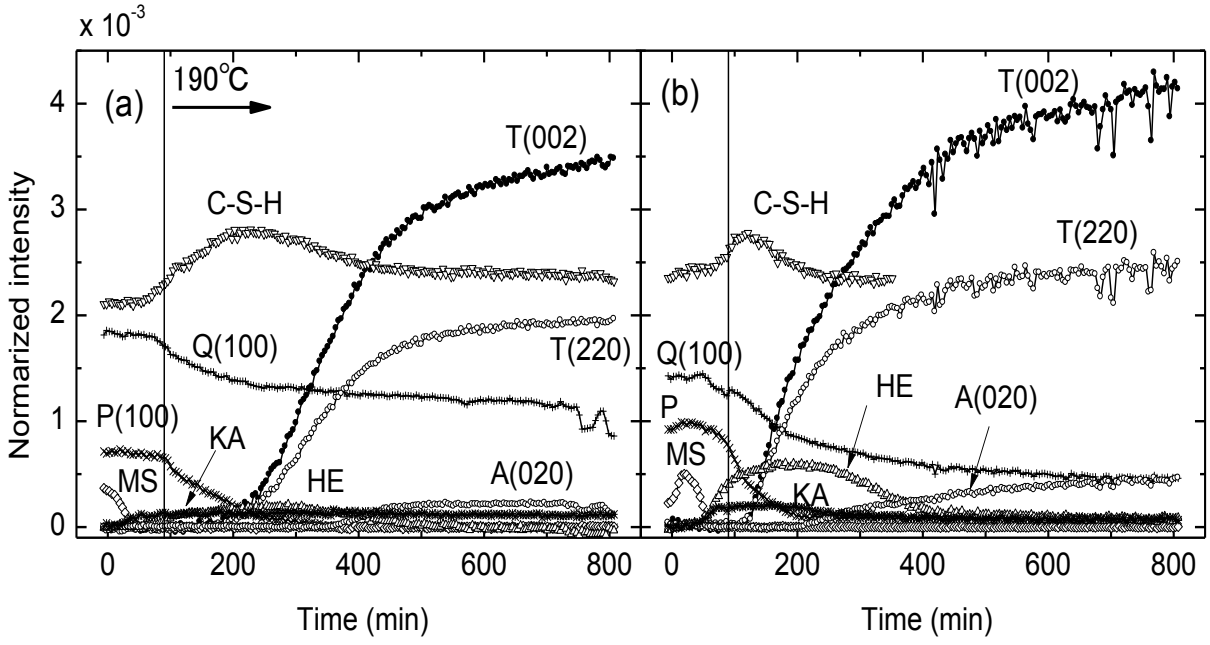

Fig. 5 Time profile of peak intensity for each major constituent during the autoclave process: (a) sample with gypsum addition and (b) sample with 4 mass % gypsum addition.

Kinetics of Tobermorite Formation

In situ XRD analysis is highly advantageous for studying hydrothermal reactions because of its high time resolution. We attempted to analyze the kinetics of the tobermorite formation reaction through the Avrami equation, which has been used to describe crystallisation involving nucleation and growth (Avrami, 1939):

$$\alpha = 1 - \exp\,[-k\,(t - t_0)^n]. \qquad (1)$$

Here, α is the degree of the reaction, k is the rate constant of the reaction, t is the reaction time, t_0 is the induction time and n is a constant that indicates the reaction mechanism. The value of n can be calculated from the slope of the –ln [ln (1 – α)] versus ln ($t - t_0$) plot (Hancock *et al.*, 1972). In this study, α was calculated from the tobermorite (222) intensity and t_0 was defined as the starting point of tobermorite formation found from Figs. 5(a) and (b). Plots of –ln [ln (1 – α)] versus ln ($t - t_0$) for both samples had high linear correlation over the α = 0.13−0.93 range, yielding n values of 2.15 for the sample without gypsum addition and 1.00 for the sample with gypsum addition. Figure 6 shows the time profiles of each sample for the calculated α values and the theoretical curves from equation (1) for the calculated n values.

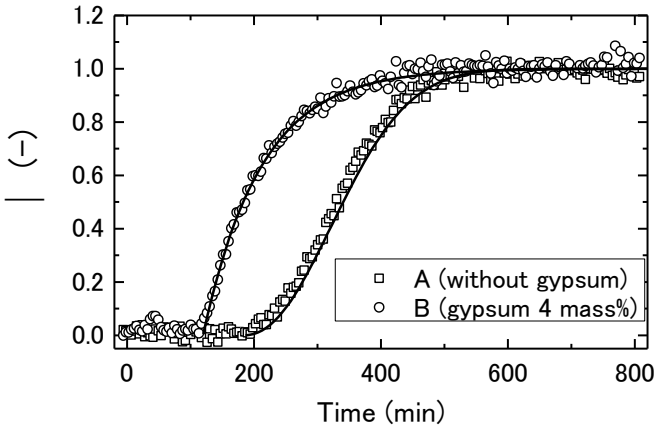

Fig. 6 Time profiles of degrees of reaction (α) calculated from the tobermorite (222) intensity and the theoretical curve from Avrami model for samples without gypsum addition and with 4 mass % gypsum addition.

The Avrami exponent n has been defined more exactly in terms of three additional constants (Brown *et al.,* 1985):

$$n = (P/S) + Q. \quad (2)$$

Here, P is the dimensionality constant for the growth of a product: P = 1 for one-dimensional growth (fibres, needles etc.), P = 2 for two-dimensional growth (plates and sheets) and P = 3 for three-dimensional growth. S is related to the rate-limiting growth mechanism: S = 1 for interface- or phase-boundary-controlled growth and S = 2 for diffusion-controlled growth. Q is a constant that indicates the nucleation rate: Q = 1 for a constant nucleation rate and Q = 0 for nucleation site saturation (zero nucleation rate). It is reasonable to assume that P/S in equation (2) is 1 in the present experiments, that is, P = 2 (plate growth) and S = 2 (diffusion-controlled process). Consequently, Q = 1.15 for the sample without gypsum and Q = 0 for the sample with gypsum addition. Therefore, all nucleation sites were saturated and tobermorite crystallized without further formation of nuclei in the system having higher sulfate concentration. On the other hand, tobermorite crystallized with nucleation in the system having lower sulfate ion concentration. The fact that the induction time was shorter and the initial formation rate was higher in the system with added gypsum supports this hypothesis. It is not clear how sulfate affect nucleation. Additional studies of this nucleation effect should be conducted.

CONCLUSION

With consideration of the effects of Al and gypsum addition, the hydrothermal formation reaction of tobermorite in the AAC process as a hydrothermally treated cement-based material has been investigated by *in situ* X-ray diffraction. Both additives clearly accelerated tobermorite formation in the AAC process. As intermediate phases, non-crystalline calcium silicate hydrate (C-S-H), hydroxylellestadite (HE), and katoite (KA) were clearly observed. It was verified that there were reaction pathways to tobermorite formation via C-S-H, KA, and HE. In the experiment on gypsum addition, the Avrami model fitted well to the calculated reaction degrees over almost the entire reaction period, and different exponent coefficients were obtained for the two systems. On the one hand, these findings suggest that the reaction proceeded in parallel with nucleation in the system having lower sulfate concentration. On the other hand, in the system with higher sulfate concentration, tobermorite began to form after nucleation had completed, and this formation continued until the reaction's end.

ACKNOWLEDGEMENTS

This study was performed with the approval of the Japanese Synchrotron Radiation Research Institute (Proposal Nos. 2008B1864, 2008B2031 and 2009B1788).

REFERENCES

Avrami, M., 1939. “Kinetics of phase change”. I, J. Chem. Phys, 7, 1103-1112.

Brown, P.W., Pommersheim, J. and Frohnsdorff, G., 1985. “A kinetic model for the hydration of tricalcium silicate”. Cem. Concr. Res., 15, 35−41.

Grutzeck, M.W. “Cellular Concrete”. *In* “Cellular Ceramics”. Wiley-VCH, Weinheim, 2005, pp.193-223.

Haas, M. “The future of AAC – from a material scienst’s point of view”. *In* “Autoclaved aerated concrete”. Taylor & Francis, London, 2005, pp.187-193.

Hancock, J.D. and Sharp, J.H., 1972. “Method of comparing solid-state kinetic data and its application to the decomposition of kaolinite, brucite, and $BaCO_3$”. J. Am. Ceram. Soc., 55, 74−77.

Kikuma, J., Tsunashima, M., Ishikawa, T., Matsuno, S., Ogaw,a A., Matsui, K. and Sato M., 2010. “In-situ time-resolved X-ray diffraction of tobermorite formation process under autoclave condition”. J. Am. Ceram. Soc., 93, 2667-2674.

Kikuma, J., Tsunashima, M., Ishikawa, T., Matsuno, S., Ogawa, A., Matsui, K. and Sato, M., 2011. “Effect of quartz particle size and water-to-solid raitio on hydrothermal synthesis of tobermorite studied by in-situ time-resolved X-ray diffraction”. J. Solid State Chem., 184, 2066-2074.

Larosa-Thompson, J.L. and Grutzeck, M.W., 1996. “C-S-H, tobermorite, and coexisting phases in the system CaO-Al_2O_3-SiO_2-H_2O”. World Cement, 27, 69-74.

Matsui,K., Kikuma J., Tsunashima M., Ishikawa T., Matsuno S., Ogawa A. and Sato M., 2011. “*In situ* time-resolved X-ray diffraction of tobermorite formation in autoclaved aerated concrete: Influence of silica source reactivity and Al addition”. Cem. Concr. Res., 41, 510-519.

Mitsuda, T., Sasaki K. and Ishida H., 1992. “Phase evolution during autoclaving process of aerated concrete”. J. Am. Ceram. Soc., 75, 1858-1863.

Sakiyama, M., Oshio Y. and Mitsuda, T., 2000. “Influence of gypsum on the hydrothermal reaction of lime-quartz system and on the strength of autoclaved calcium silicate product”. J. Soc. Inorganic Mater. Jpn., 7, 685−691.